

Nonadiabatic single-qubit quantum Otto engine

Andrea Solfanelli,^{1,2} Marco Falsetti,¹ and Michele Campisi^{1,2}

¹*Department of Physics and Astronomy, University of Florence,
Via Sansone 1, I-50019, Sesto Fiorentino (FI), Italy.*

²*INFN Sezione di Firenze, via G. Sansone 1, I-50019, Sesto Fiorentino (FI), Italy.*

According to Clausius formulation of the second law of thermodynamics, for any thermal machine withdrawing heats $Q_{1,2}$ from two heat reservoirs at temperatures $T_{1,2}$, it holds $Q_1/T_1 + Q_2/T_2 \leq 0$. Combined with the observation that the quantity $Q_1 + Q_2$ is the work W done by the system, that inequality tells that only 4 possible operation modes are possible for the thermal machine, namely heat engine [E], refrigerator [R], thermal accelerator [A] and heater [H]. We illustrate their emergence in the finite time operation of a quantum Otto engine realised with a single qubit. We first focus on the ideal case when isothermal and thermally-insulated strokes are well separated, and give general results as well as results pertaining to the specific finite-time Landau-Zener dynamics. We then present realistic results pertaining to the solid-state experimental implementation proposed by Karimi and Pekola [Phys. Rev. B **94** (2016) 184503]. That device is non-adiabatic both in the quantum mechanical sense and in the thermodynamical sense. Oscillations in the power extracted from the baths due to coherent LZ tunnelling at too low temperatures are observed that might hinder the robustness of the operation of the device against experimental noise on the control parameters.

I. INTRODUCTION

One of the cornerstones of thermodynamics is Clausius inequality:

$$\sum_i \frac{Q_i}{T_i} \leq 0, \quad (1)$$

where Q_i are the energies that a central system undergoing a cyclic transformation withdraws from a set of surrounding heat baths at temperatures T_i . In the continuum limit it gives the celebrated expression $\oint \delta Q/T \leq 0$. Noting that the equal sign holds when the cycle is reversible, led Clausius to naturally introduce the state function S such that $dS = \delta Q_{\text{rev}}/T$, with Q_{rev} being the heat exchanged during a reversible transformation, and the property that $S(B) - S(A) \geq \int_A^B \delta Q/T$. S is the entropy [1].

For the simplest case of a central system interacting with two baths only and a work source, the above Eq. (1), combined with the first law of thermodynamics, gives the following conditions

$$\beta_1 Q_1 + \beta_2 Q_2 \leq 0 \quad (2)$$

$$Q_1 + Q_2 = W, \quad (3)$$

where W is the work delivered to the work source and β_i are the baths inverse thermal energies $\beta_i = (kT_i)^{-1}$, and k is Boltzmann's constant. Looking at the system as a thermal machine, depending on the signs of Q_1, Q_2, W it may realise various operation modes. Basic mathematics show that the above constraints are simultaneously compatible only with 4 (out of a total of $8 = 2^3$) operation modes, see Appendix A. Setting, without loss of

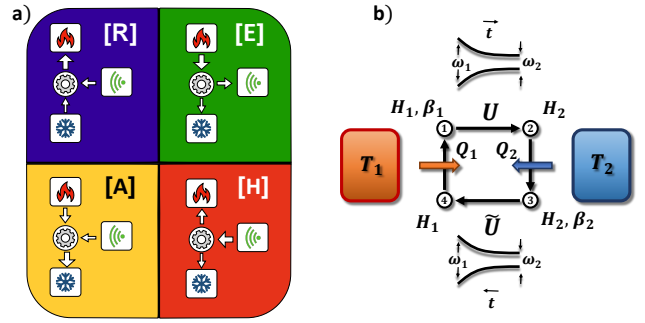


FIG. 1: Panel a) The four possible operation modes for a device working with two reservoirs. Panel b) Sketch of a single-qubit based quantum Otto engine cycle.

generality, the convention $\beta_1 < \beta_2$, these are

$$[R]: Q_1 \leq 0 \quad Q_2 \geq 0 \quad W \leq 0 \quad (4)$$

$$[E]: Q_1 \geq 0 \quad Q_2 \leq 0 \quad W \geq 0 \quad (5)$$

$$[A]: Q_1 \geq 0 \quad Q_2 \leq 0 \quad W \leq 0 \quad (6)$$

$$[H]: Q_1 \leq 0 \quad Q_2 \leq 0 \quad W \leq 0, \quad (7)$$

where [E] denotes energy extraction (heat engine), [R] denotes refrigerator, [A] denotes thermal accelerator, and [H] denotes heater [2]. They are illustrated in Fig. 1, panel a).

In this work we illustrate how the four operations emerge in a quantum Otto engine operating in finite time.

II. SINGLE-QUBIT QUANTUM OTTO ENGINE

We consider an engine consisting of a single qubit undergoing a four stroke cycle. See Fig. 1 panel b). We

assume the qubit is initially at thermal equilibrium at temperature T_1 . In the first stroke the qubit undergoes an evolution where its resonant frequency changes from a value ω_1 to a value ω_2 . In the second stroke the qubit at fixed resonant frequency ω_2 interacts with the thermal bath 2 so as to reach temperature T_2 . In the third stroke the qubit undergoes a reversed evolution where its resonant frequency changes from the value ω_2 to the value ω_1 . In the fourth stroke the qubit at fixed resonant frequency ω_1 interacts with the thermal bath 1 so as to reach temperature T_1 , thus closing the cycle.

The first and third strokes are adiabatic in a thermodynamic sense (namely they occur in thermal isolation), but are not necessarily adiabatic in the quantum-mechanical sense, namely, during the evolution quantum transitions may occur.

The unitary dynamics U occurring in the first stroke are generated by a generic time-dependent spin-1/2 Hamiltonian $H(t)$, according to the rules of quantum mechanics:

$$H(t) = x(t)\sigma_x + y(t)\sigma_y + z(t)\sigma_z, \quad t \in [t_1, t_2], \quad (8)$$

$$U = \text{T exp} \left[-(i/\hbar) \int_{t_1}^{t_2} H(s) ds \right], \quad (9)$$

where T exp denotes the time-ordered exponential, t_1 and t_2 are initial and final times of the stroke, $\sigma_{x,y,z}$ denote Pauli operators, and $x(t), y(t), z(t)$ are generic time dependent real coefficients. The qubit level spacings at the beginning and end of the first stroke are give by the expressions:

$$\hbar\omega_1 = 2\sqrt{x^2(t_1) + y^2(t_1) + z^2(t_1)}, \quad (10)$$

$$\hbar\omega_2 = 2\sqrt{x^2(t_2) + y^2(t_2) + z^2(t_2)} \quad (11)$$

The unitary dynamics \tilde{U} occurring in the third stroke are generated by the time-dependent Hamiltonian realising the ‘‘backward’’ protocol

$$\tilde{H}(t) = H(t_2 + t_1 - t), \quad t \in [t_1, t_2] \quad (12)$$

$$\tilde{U} = \text{T exp} \left[-(i/\hbar) \int_{t_1}^{t_2} \tilde{H}(s) ds \right]. \quad (13)$$

We assume that at each time $t \in [t_1, t_2]$ the Hamiltonian $H(t)$ is invariant under the action of some anti-unitary operator K , $H(t) = KH(t)^\dagger K^\dagger$ [17]. Under that assumption it is [3]:

$$\tilde{U} = KU^\dagger K^\dagger. \quad (14)$$

For simplicity we introduce the notation:

$$H_1 = H(t_1) = \tilde{H}(t_2) \quad (15)$$

$$H_2 = H(t_2) = \tilde{H}(t_1). \quad (16)$$

Let ρ_i and E_i denote the state of the qubit at the beginning of stroke i and its according energy expectation value. By the thermalisation assumption and Eqs.

(9,13), it is:

$$\begin{aligned} \rho_1 &= e^{-\beta_1 H_1} / Z_1, & E_1 &= \text{Tr} \rho_1 H_1 \\ \rho_2 &= U \rho_1 U^\dagger, & E_2 &= \text{Tr} \rho_2 H_2 \\ \rho_3 &= e^{-\beta_2 H_2} / Z_2, & E_3 &= \text{Tr} \rho_3 H_2 \\ \rho_4 &= \tilde{U} \rho_3 \tilde{U}^\dagger, & E_4 &= \text{Tr} \rho_4 H_1, \end{aligned} \quad (17)$$

where $Z_i = \text{Tr} e^{-\beta_i H_i}$ is the canonical partition function.

The thermodynamics of the engine is fully characterised by the heats Q_1, Q_2 withdrawn from the baths 1, 2 during the thermalisation steps which, under the assumption of weak qubit bath coupling, equal the energies gained by the qubit during those strokes namely:

$$Q_2 = E_3 - E_2 \quad (18)$$

$$Q_1 = E_1 - E_4. \quad (19)$$

Since E_1 and E_3 are thermal expectations they can be readily expressed as:

$$E_1 = -\frac{\hbar\omega_1}{2} \tanh \left(\frac{\beta_1 \hbar\omega_1}{2} \right) \quad (20)$$

$$E_3 = -\frac{\hbar\omega_2}{2} \tanh \left(\frac{\beta_2 \hbar\omega_2}{2} \right). \quad (21)$$

For E_2 we obtain:

$$E_2 = \frac{\sum_{i,j} \varepsilon_i^{(2)} e^{-\beta_1 \varepsilon_j^{(1)}} |\langle \psi_i^{(2)} | U | \psi_j^{(1)} \rangle|^2}{2 \cosh(\beta_1 \hbar\omega_1/2)}, \quad (22)$$

where $|\psi_i^{(r)}\rangle, \varepsilon_i^{(r)}$, $i, r = 1, 2$ are the eigenvectors and corresponding eigenvalues of H_r : $H_r |\psi_i^{(r)}\rangle = \varepsilon_i^{(r)} |\psi_i^{(r)}\rangle$. Choosing the label $i = 1, 2$ for the ground and excited states respectively, it is $\varepsilon_1^{(r)} = -\hbar\omega_r/2, \varepsilon_2^{(r)} = +\hbar\omega_r/2$.

Note that the 2×2 square matrix $P_{ij} = |\langle \psi_i^{(2)} | U | \psi_j^{(1)} \rangle|^2$ is doubly stochastic [4], namely $0 \leq P_{ij} \leq 1, \sum_i P_{ij} = \sum_j P_{ij} = 1$. This immediately implies that one of its elements is sufficient to determine all of them, and that the matrix is symmetric: if $P_{11} \doteq P$, then $P_{12} = P_{21} = 1 - P$, and $P_{22} = P$. Then E_2 reads

$$E_2 = \frac{\hbar\omega_2}{2} \tanh \left(\frac{\beta_1 \hbar\omega_1}{2} \right) (1 - 2P), \quad (23)$$

where P contains all relevant information pertaining to the degree of adiabaticity of the sweep. In the adiabatic limit where there occur no transitions among the instantaneous energy eigenstates, we have $P \rightarrow 1$ and $E_2 \rightarrow E_1 \omega_2 / \omega_1$ in accordance with the energy spectrum getting dilated/contracted by a factor ω_2 / ω_1 .

Similarly, for the calculation of E_4 we obtain

$$E_4 = \frac{\sum_{i,j} \varepsilon_i^{(1)} e^{-\beta_2 \varepsilon_j^{(2)}} |\langle \psi_i^{(1)} | \tilde{U} | \psi_j^{(2)} \rangle|^2}{2 \cosh(\beta_2 \hbar\omega_2/2)}. \quad (24)$$

Using Eq. (13) and the property $\langle u | KAK^\dagger | w \rangle = \langle u | A | w \rangle^*$ (with A a linear operator, and K an anti-linear

operator) [5] we get

$$\begin{aligned} |\langle \psi_i^{(1)} | \tilde{U} | \psi_j^{(2)} \rangle|^2 &= |\langle \psi_i^{(1)} | K U^\dagger K^\dagger | \psi_j^{(2)} \rangle|^2 = \\ |\langle \psi_i^{(1)} | U^\dagger | \psi_j^{(2)*} \rangle|^2 &= |\langle \psi_j^{(2)} | U | \psi_i^{(1)} \rangle|^2 = P_{ji} = P_{ij}, \end{aligned} \quad (25)$$

hence

$$E_4 = \frac{\hbar\omega_1}{2} \tanh\left(\frac{\beta_2\hbar\omega_2}{2}\right) (1 - 2P). \quad (26)$$

Summing up:

$$Q_1 = -\frac{\hbar\omega_1}{2} \left[\tanh\left(\frac{\beta_1\hbar\omega_1}{2}\right) + \tanh\left(\frac{\beta_2\hbar\omega_2}{2}\right) (1 - 2P) \right] \quad (27)$$

$$Q_2 = -\frac{\hbar\omega_2}{2} \left[\tanh\left(\frac{\beta_2\hbar\omega_2}{2}\right) + \tanh\left(\frac{\beta_1\hbar\omega_1}{2}\right) (1 - 2P) \right] \quad (28)$$

$$\begin{aligned} W &= -\frac{\hbar}{2} \tanh\left(\frac{\beta_1\hbar\omega_1}{2}\right) [\omega_1 + \omega_2(1 - 2P)] \\ &\quad - \frac{\hbar}{2} \tanh\left(\frac{\beta_2\hbar\omega_2}{2}\right) [\omega_1(1 - 2P) + \omega_2]. \end{aligned} \quad (29)$$

The transition probability P contains information pertaining to the qubit dynamics during the unitary strokes, as such it is a functional of $\{x(t), y(t), z(t)\}$, which we leave unspecified for now. It is trivial to note that all energy exchanges are increasing functions of P and are maximal in the adiabatic limit $P = 1$. Departure from that limit means smaller exchanges. As we shall see below it also means smaller thermodynamic efficiencies.

It is not difficult to see that, with $Q_{1,2}$ as in Eq. (27,28) it is $\beta_1 Q_1 + \beta_2 Q_2 \leq 0$ in accordance with Eq. (2), see Appendix B.

Since the above expressions are linear in P , it is easy to find the values of P , call them P_{Q_1}, P_{Q_2}, P_W for which Q_1, Q_2 and W , respectively, become null, and therefore mark their sign reversal:

$$P_{Q_1} = \frac{1}{2} \left[1 + \frac{\tanh(\beta_1\hbar\omega_1/2)}{\tanh(\beta_2\hbar\omega_2/2)} \right] \quad (30)$$

$$P_{Q_2} = \frac{1}{2} \left[1 + \frac{\tanh(\beta_2\hbar\omega_2/2)}{\tanh(\beta_1\hbar\omega_1/2)} \right] \quad (31)$$

$$P_W = \frac{1}{2} \left[1 + \frac{\hbar\omega_1 \tanh(\beta_1\hbar\omega_1/2) + \hbar\omega_2 \tanh(\beta_2\hbar\omega_2/2)}{\hbar\omega_2 \tanh(\beta_1\hbar\omega_1/2) + \hbar\omega_1 \tanh(\beta_2\hbar\omega_2/2)} \right] \quad (32)$$

Figure 2 shows the curves P_{Q_1}, P_{Q_2}, P_W , as a function of ω_2/ω_1 , for various fixed values of $\beta_1\hbar\omega_1, \beta_2\hbar\omega_1$. Crossing one curve means reversing the sign of the according quantity, therefore the curves draw the boundaries of the regions of distinct operation modes. As expected there are only four regions, corresponding each to one of the four allowed operation modes described above, which we have filled with different colours.

A few observations are in order. First, the regions, as plotted in the $(\omega_2/\omega_1, P)$ plane are connected. We note

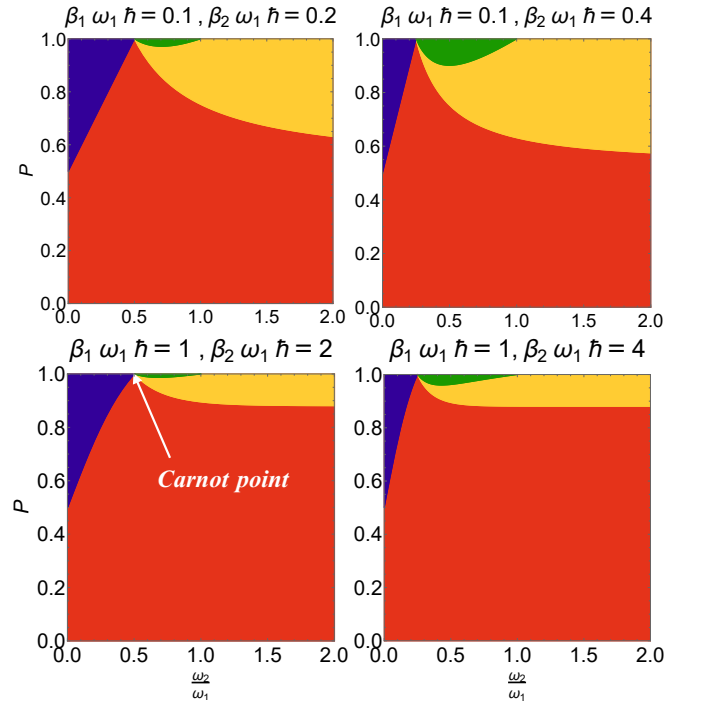


FIG. 2: Operation regions in the $(\omega_2/\omega_1, P)$ plane. Blue=[R]. Red=[H]. Green = [E]. Yellow = [A], in accordance with the color convention in Fig 1 a). Moving downward the ratio β_1/β_2 is fixed, and β_2 increases. Moving to the right β_1 is fixed, while β_1/β_2 decreases. The Carnot point ($\omega_2/\omega_1 = \beta_1/\beta_2, P = 1$) where all operations coincide is indicated in panel c) only.

that for $P < 1/2$ only the [H] operation is possible: from Eqs. (27, 28) one can immediately see that for $P < 1/2$ it is $Q_1 \leq 0, Q_2 \leq 0$. As P gets larger and larger, above the value $1/2$ the [H]-region shrinks until it reduces to a single point, which is in fact the Carnot point (characterised by $\omega_2/\omega_1 = \beta_1/\beta_2$ and $P = 1$) where all operations coincide, and actually nothing happens (i.e., all exchanged energies are null). For $P = 1$, corresponding to the quasi-static (i.e., adiabatic in the quantum-mechanical sense) limit, only [R], [E] and [A] are possible, with [R] occurring for $\omega_2/\omega_1 \leq \beta_1/\beta_2$, [E] occurring for $\beta_1/\beta_2 \leq \omega_2/\omega_1 \leq 1$, and [A] occurring for $\omega_2/\omega_1 \geq 1$. As P decreases from the value 1, the according intervals become smaller at the expense of an enlarging [H] interval.

Note that $P_{Q_2} \rightarrow 1/2$ as $\hbar\omega_2 \rightarrow 0$, which gives the [R] region a triangular-like shape, with one side of fixed length and the other side with a size that gets smaller and smaller as the ratio β_1/β_2 decreases. That reflects the fact that, at fixed hot temperature T_1 , extracting heat from the cold bath becomes more and more difficult as T_2 decreases. Note also that contextually, the [E] region would expand, reflecting the fact that it is easier to deliver positive work, when there is a larger thermal gradient. The region [H] is the biggest in the $(\omega_2/\omega_1, P)$ plane, in accordance with the intuitive idea that dump-

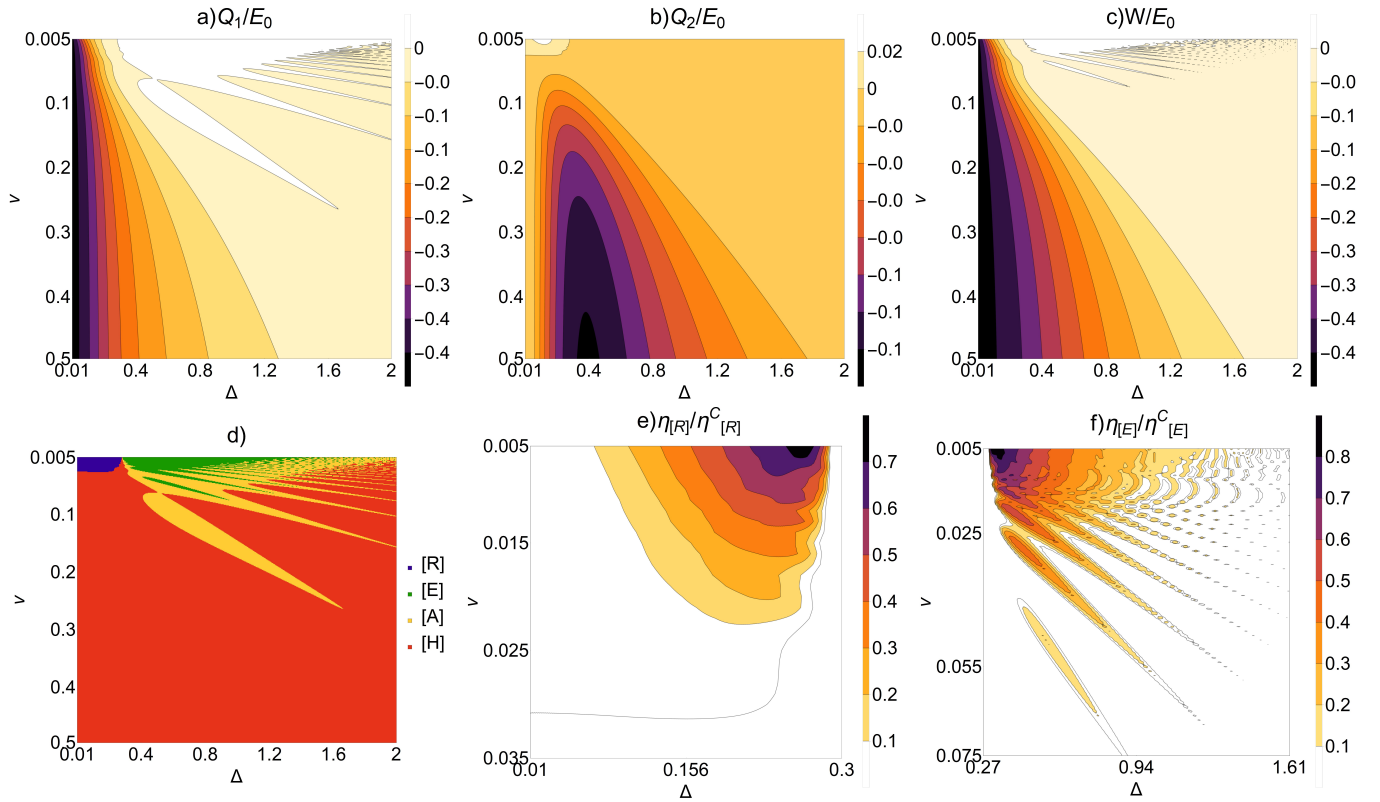


FIG. 3: Thermodynamics of the Landau-Zener-Stückelberg-Majorana quantum Otto engine as function of the nondimensional parameters v, Δ at fixed $v\tau = 1/2$. Panel a): Heat withdrawn from resistor 1 in one cycle. Panel b) Heat withdrawn from resistor 2 in one cycle. Panel c) Work output. Panel d) Operation regions: Blue=[R]; Red=[H]; Green = [E]; Yellow = [A]. Panel e): Rescaled refrigeration efficiency $\eta_{[R]}/\eta_{[R]}^C$. Panel f): Rescaled heat engine efficiency $\eta_{[E]}/\eta_{[E]}^C$. The temperature ratio is $T_1/T_2 = \beta_2/\beta_1 = 2$, while $\beta_1 E_0 = 10/3$. The Carnot point is accordingly at $v = 0, \Delta = 1/\sqrt{12} \simeq 0.29$, and the Carnot efficiencies are $\eta_{[E]}^C = 1/2$ and $\eta_{[R]}^C = 1$.

ing heat in both baths is the generally the easiest thing to accomplish.

As anticipated, transitions are responsible for drops in the thermodynamic efficiency. To see that, consider the [E] regime, where $Q_1 \geq 0, Q_2 \leq 0$. The thermodynamic efficiency $\eta_{[E]} = W/Q_1 = 1 + Q_2/Q_1$ reads:

$$\eta_{[E]} = 1 + \frac{\omega_2 \tanh(\beta_2 \hbar \omega_2 / 2) + \tanh(\beta_1 \hbar \omega_1 / 2)(1 - 2P)}{\omega_1 \tanh(\beta_1 \hbar \omega_1 / 2) + \tanh(\beta_2 \hbar \omega_2 / 2)(1 - 2P)} \quad (33)$$

Note that both numerator and denominator in the equation above decrease with increasing P , so while the numerator (i.e., $-2Q_2/\hbar$, which is positive) becomes less positive, the denominator (i.e., $-2Q_1/\hbar$ which is negative) becomes more negative. Accordingly, the absolute value of the ratio (which is a negative number) decreases with increasing P , implying that $\eta_{[E]}$ is an increasing function of P . Similarly one can see that the coefficient of performance in the [R]-operation decreases with P . Accordingly best thermodynamic performances are achieved in the quasi-static limit, where the quasi-static Otto efficiencies [6, 7] occur: $\eta_{[E]}^{qs} = 1 - \omega_2/\omega_1$

and $\eta_{[R]}^{qs} = 1/(\omega_1/\omega_2 - 1)$, which in turn increase and tend to the Carnot efficiencies $\eta_{[E]}^C = 1 - \beta_1/\beta_2$, $\eta_{[R]}^C = 1/(\beta_2/\beta_1 - 1)$ as one gets close to the Carnot point. However, as pointed out above the absolute value of the exchanged energies go to zero at the Carnot point.

III. LANDAU-ZENER-STÜCKELBERG-MAJORANA DYNAMICS

We now focus on the specific case of the Landau-Zener-Stückelberg-Majorana [8–11] evolution,

$$x(t) = \delta, \quad y(t) = 0, \quad z(t) = ut \quad (34)$$

Note that, if adopting the $\{\sigma_z\}$ representation where the Pauli matrices σ_x, σ_z are real, the according Hamiltonian is invariant under the anti-unitary complex conjugation $K_{\{\sigma_z\}}$ relative to that representation [5], so we are within the assumptions stated above.

The transition probability P can be expressed in this case in terms of the problem parameters (δ, u, t_1, t_2) by means of parabolic cylinder functions, as described in

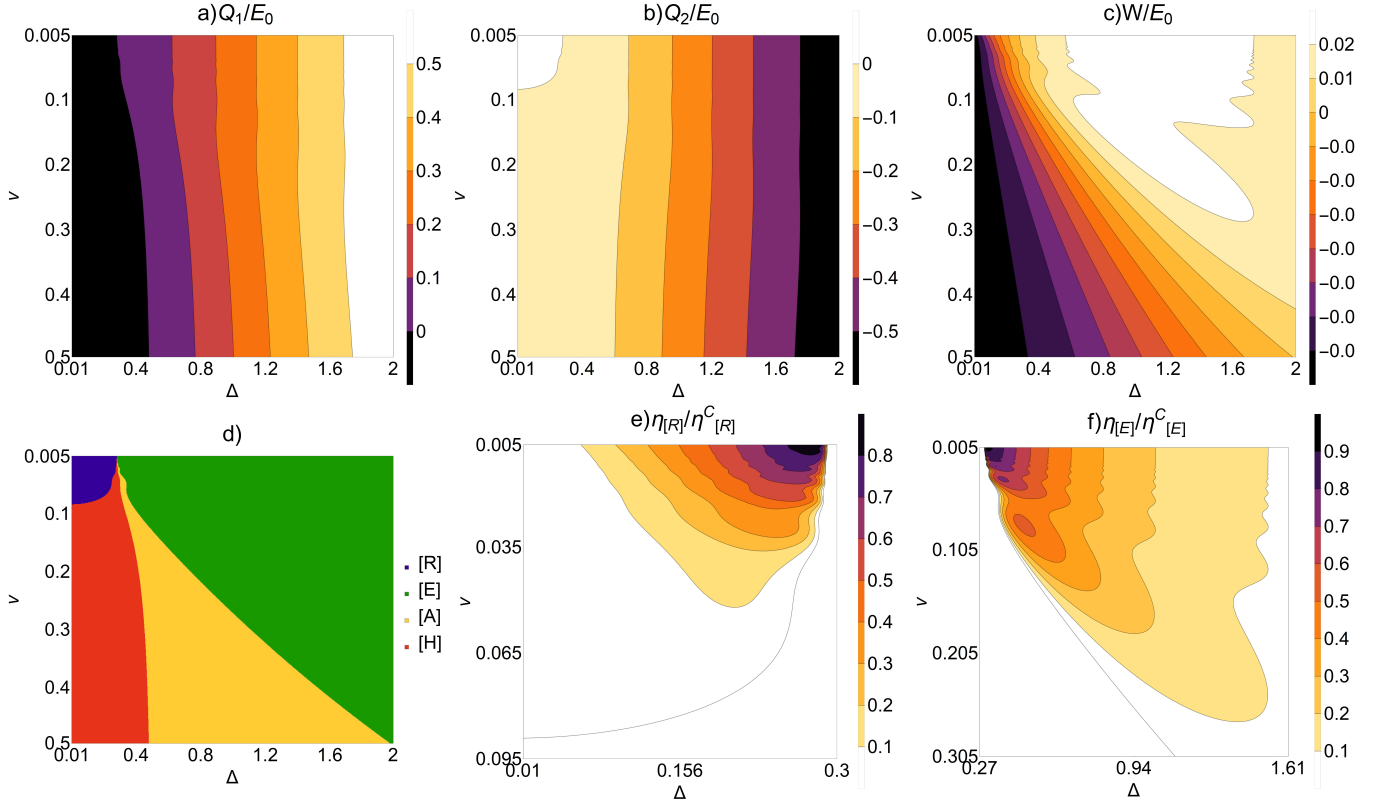


FIG. 4: Same as Fig. 3 but for $\beta_1 E_0 = 1/3$.

[12]. The unitary evolution in the $\{\sigma_z\}$ representation reads:

$$U_{11}(t_2, t_1) = U_{22}^*(t_2, t_1) = \frac{\Gamma(1 - i\frac{\delta^2}{2u})}{\sqrt{2\pi}} \times \left[D_{i\frac{\delta^2}{2u}}(t_2\sqrt{2u}e^{-i\pi/4})D_{i\frac{\delta^2}{2u}-1}(t_1\sqrt{2u}e^{i3\pi/4}) + D_{i\frac{\delta^2}{2u}}(t_2\sqrt{2u}e^{i3\pi/4})D_{i\frac{\delta^2}{2u}-1}(t_1\sqrt{2u}e^{-i\pi/4}) \right] \quad (35)$$

$$U_{12}(t_2, t_1) = -U_{21}^*(t_2, t_1) = \frac{\Gamma(1 - i\frac{\delta^2}{2u})e^{i\pi/4}}{\delta\sqrt{\pi/u}} \times \left[-D_{i\frac{\delta^2}{2u}}(t_2\sqrt{2u}e^{-i\pi/4})D_{i\frac{\delta^2}{2u}}(t_1\sqrt{2u}e^{i3\pi/4}) + D_{i\frac{\delta^2}{2u}}(t_2\sqrt{2u}e^{i3\pi/4})D_{i\frac{\delta^2}{2u}}(t_1\sqrt{2u}e^{-i\pi/4}) \right] \quad (36)$$

where $U_{ij} = \langle \phi_i | U | \phi_j \rangle$ and $|\phi_1\rangle, |\phi_2\rangle$ denote the spin-down and spin-up eigenvectors of σ_z , respectively; $D_\nu(z)$ denotes the parabolic cylinder D-function and $\Gamma(z)$ is the Gamma function [13]. Denoting with $\mathbf{U}^{ad}(t_2, t_1)$ the time evolution matrix expressed in the time varying instantaneous Hamiltonian eigenbasis, it is [12]:

$$\mathbf{U}^{ad}(t_2, t_1) = \mathbf{R}^T(t_2) \cdot \mathbf{U}(t_2, t_1) \cdot \mathbf{R}(t_1), \quad (37)$$

where $\mathbf{U}(t_2, t_1)$ is the time evolution matrix expressed in the $\{\sigma_z\}$ eigenbasis, $\mathbf{R}(t_r)$, $r = 1, 2$ is the rotation that

changes the basis from adiabatic (eigenstates of H_r) to diabatic (eigenstates of σ_z):

$$\mathbf{R}(t) = \begin{pmatrix} \cos \vartheta(t) & \sin \vartheta(t) \\ -\sin \vartheta(t) & \cos \vartheta(t) \end{pmatrix}, \quad \vartheta(t) = \frac{1}{2} \arctan \frac{\delta}{ut}. \quad (38)$$

The probability P then reads $P = |\mathbf{U}_{11}^{ad}(t_2, t_1)|^2$.

Introducing a qubit energy scale E_0 , we define the nondimensional level spacing $\Delta = \delta/E_0$, nondimensional sweep rate, $v = \hbar h/E_0^2$ and nondimensional time $s = E_0 t/\hbar$.

In the following we focus on a sweep between nondimensional time $s_1 = -\tau$ (with $\tau > 0$) and $s_2 = 0$, corresponding to $\hbar\omega_1 = 2E_0\sqrt{\Delta^2 + (v\tau)^2}$, $\hbar\omega_2 = 2\Delta E_0$. Note that with this choice it is $\omega_2 \leq \omega_1$, hence we are exploring the region where all four operations may occur (for $\omega_2 \geq \omega_1$ only [H] and [A] may occur). Figures 3,4 show, for fixed temperature ratio β_2/β_1 and different β_1 , the plots of $Q_1/E_0, Q_2/E_0, W/E_0$, the regions of operations and the rescaled thermodynamic efficiencies $\eta_{[R]}/\eta_{[R]}^C$ and $\eta_{[E]}/\eta_{[E]}^C$, as a function of v, Δ , for fixed $\alpha = v\tau$. The limit $v \rightarrow 0$ ($\tau \rightarrow \infty$) corresponds to the adiabatic limit. Note how the low temperature plots (Fig. 3) present oscillations in Δ and v , which result in a breakdown of the connectedness of the operation regions. These are a consequence of the well-known oscillations that charac-

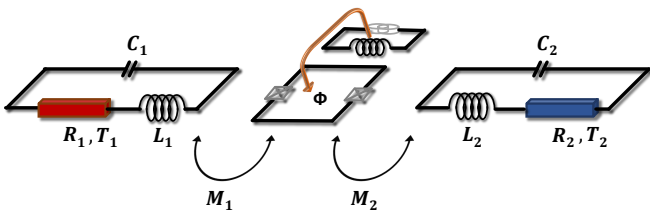


FIG. 5: Circuit scheme of the Quantum Otto Engine of Karimi and Pekola [15].

terise LZSM transitions in finite time [12, 14]. Note that they do not appear in the higher temperature plots (Fig. 4). Note how, as Δ increases the intervals of v where [A] occurs shrink, and in practice only [H] occurs in the $\Delta \rightarrow \infty$ limit. This is well visible in low temperature plot (Fig. 3 panel d), and would be visible at higher temperatures (Fig. 4 panel d), if one would enlarge the Δ -axis end-scale accordingly. This behaviour can be understood by looking at Eq. (30). When $\Delta \rightarrow \infty$ both ω_1 and ω_2 go to infinity, hence the reversal point P_{Q_1} goes to 1, meaning that only at $P = 1$ (that is in the slow limit $v \rightarrow 0$), [A] can occur. Physically the reason is that when Δ is very large, almost all qubit population is in the ground state at the beginning of an adiabatic stroke, hence the qubit jumping-up during the adiabatic stroke has an overwhelmingly larger probability than jumping-down. Accordingly the probability of releasing energy to the bath in the subsequent thermalisation stroke is overwhelmingly larger than the probability of withdrawing it.

IV. THE QUANTUM OTTO ENGINE OF KARIMI AND PEKOLA

We consider the solid state implementation of a quantum Otto engine presented by Karimi and Pekola [15] whereby a superconducting qubit is coupled to two resistors $R_j, j = 1, 2$ each kept at temperature T_j (inverse thermal energy $\beta_j = 1/(kT_j)$) and embedded each into an RLC circuit with resonant frequency $\omega_{LC,j} = 1/\sqrt{L_j C_j}$ with L_j, C_j the j -th circuit inductance and capacitance, respectively. The coupling between the qubit and resistor R_j is achieved by tuning the qubit level spacing to $\omega_{LC,j}$. Control over the qubit level spacing is provided through the control over the magnetic flux, Φ , that threads the qubit, and is generated by a nearby inductor. The Otto engine is then realised by bringing the qubit in tune with the two LRC circuits, alternatively, see Fig. 5. This smart strategy allows, with the manipulation of a single parameter, to realise both the compression and dilation of the energy spectrum, and the switching of the qubit-baths interactions.

The qubit Hamiltonian reads:

$$H = -E_0 \Delta \sigma_x - E_0 q(t) \sigma_z, \quad (39)$$

with

$$q(t) = \frac{1 + \cos(2\pi f t)}{4}. \quad (40)$$

Accordingly the qubit level spacing periodically oscillates between the maximal value $\hbar\omega_1 = 2E_0\sqrt{\Delta^2 + 1/4}$ and the minimal value $\hbar\omega_2 = 2E_0\Delta$, where it is in resonance respectively with the hot and cold bath. Recall that Δ is a dimensionless quantity, while E_0 is an energy.

At variance with the idealised situation described in Sec.III, in this case strokes 1 and 3 are not perfectly separated from the thermalisation strokes 2 and 4. Accordingly, they cannot be described by means of unitary evolution. Note also that the qubit remains in contact with the baths for a finite time which might not result in its full thermalisation. Following Karimi and Pekola [15], we describe the dynamics of the open qubit, encompassing both the interaction with the resistors and the time-dependent driving, by means of the standard quantum master equation reading, in the instantaneous qubit energy eigenbasis:

$$\dot{\rho}_{gg}(t) = -\frac{\Delta}{q^2(t) + \Delta^2} \dot{q}(t) \Re[\rho_{ge}(t) e^{i\phi(t)}] - \Gamma_{\Sigma} \rho_{gg}(t) + \Gamma_{\downarrow} \quad (41)$$

$$\dot{\rho}_{ge}(t) = \frac{\Delta}{q^2(t) + \Delta^2} \dot{q}(t) (\rho_{gg}(t) - 1/2) e^{-i\phi(t)} - \Gamma_{\Sigma} \rho_{ge}(t)/2 \quad (42)$$

where $\phi(t) = \int_0^t \omega(t') dt'$ is a dynamical phase determined by the instantaneous level spacing $\hbar\omega(t) = 2E_0\sqrt{q^2(t) + \Delta^2}$; Γ_{\downarrow} denotes jump down transition rate of the qubit caused by the interaction with the two baths, i.e., $\Gamma_{\downarrow} = \Gamma_{\downarrow,1} + \Gamma_{\downarrow,2}$, with $\Gamma_{\downarrow,i}$ the jump down transition rate caused by bath i ; $\Gamma_{\Sigma} = \sum_{j=1}^2 (\Gamma_{\downarrow,j} + \Gamma_{\uparrow,j})$ being the sum of all transition rates caused by all the baths.

The transition rates can be calculated by means of the Fermi golden rule leading to the expression [15]:

$$\Gamma_{\downarrow(\uparrow),j} = \frac{E_0^2 M_j^2}{\hbar^2 \Phi_0^2} \frac{\Delta^2}{q^2 + \Delta^2} S_{I,j}(\pm\omega) \quad (43)$$

where $S_{I,j}(\omega) = |R_j[1 + Q_j^2(\omega/\omega_{LC,j} - \omega_{LC,j}/\omega)]|^{-2} S_{V,j}(\omega)$ is the unsymmetrized noise spectrum of LRC circuit j expressed in terms of its resonance frequency $\omega_{LC,j} = 1/\sqrt{L_j C_j}$, quality factor $Q_j = \sqrt{L_j C_j}/R_j$ and voltage noise across the resistor, $S_{V,j}(\omega) = 2R_j \hbar\omega / (1 - e^{-\beta_j \hbar\omega})$. Here M_j is the mutual inductance between the qubit and the j -th RLC circuit, and $\Phi_0 = h/2e$ is the flux quantum (e denotes the electron charge and h is Planck's constant).

The power extracted from resistor j by the qubit reads [15]

$$\mathcal{P}_i(t) = -E(t) (\rho_{ee} \Gamma_{\downarrow,j} - \rho_{gg} \Gamma_{\uparrow,j}). \quad (44)$$

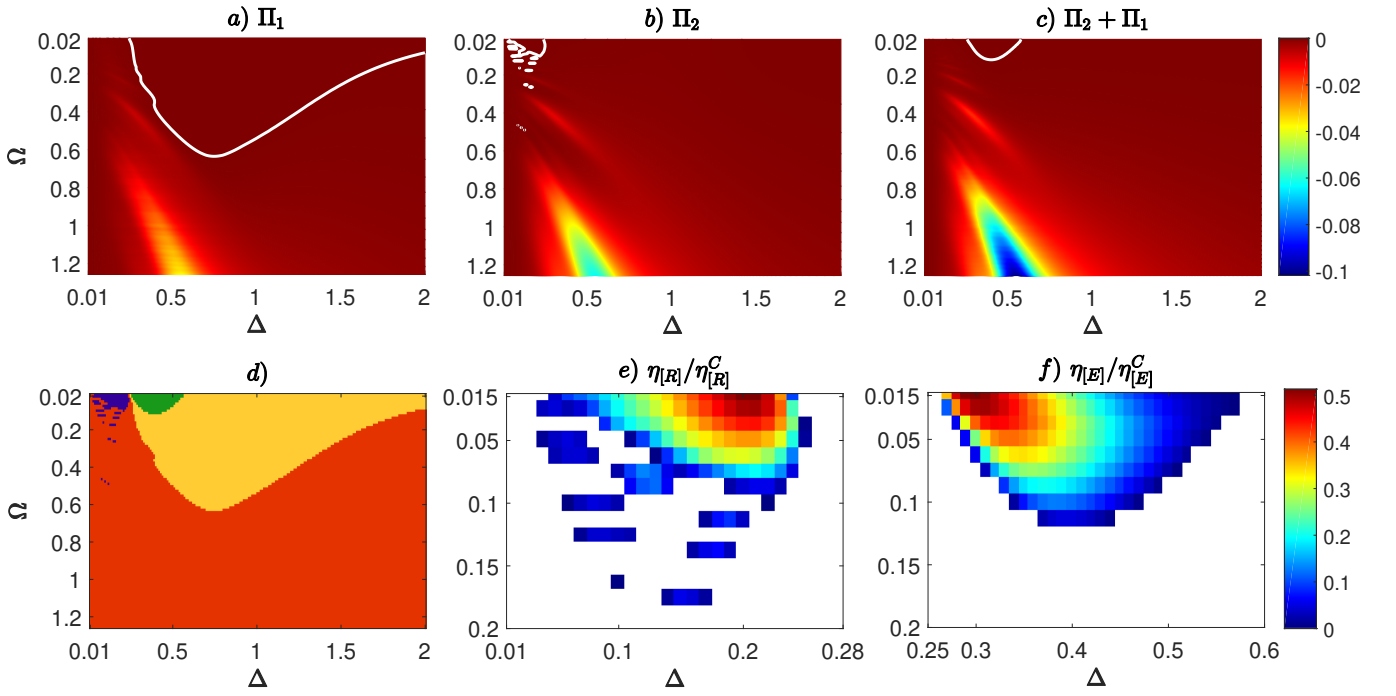


FIG. 6: Thermodynamics of the quantum Otto engine of Karimi and Pekola [15] as function of the parameters Ω, Δ . Panel a): Power withdrawn from resistor 1. Panel b): Power withdrawn from resistor 2. Panel c): Power output. White curves denote the zero-level contours. Panel d): Operation regions: Blue=[R]; Red=[H]; Green = [E]; Yellow = [A], in accordance with the convention set in Fig. 1a). Panel e): Rescaled refrigeration efficiency $\eta_{[R]}/\eta_{[R]}^C$. Panel f): Rescaled heat engine efficiency $\eta_{[E]}/\eta_{[E]}^C$. The temperature ratio is $T_1/T_2 = \beta_2/\beta_1 = 2$, while $\beta_1 E_0 = 10/3$. The Carnot point is accordingly at $\Omega = 0, \Delta = 1/\sqrt{12} \simeq 0.29$, and the Carnot efficiencies are $\eta_{[E]}^C = 1/2$ and $\eta_{[R]}^C = 1$. Following Ref. [15] the quality factor of both LRC circuits is set to the value $\mathcal{Q}_1 = \mathcal{Q}_2 = 30$.

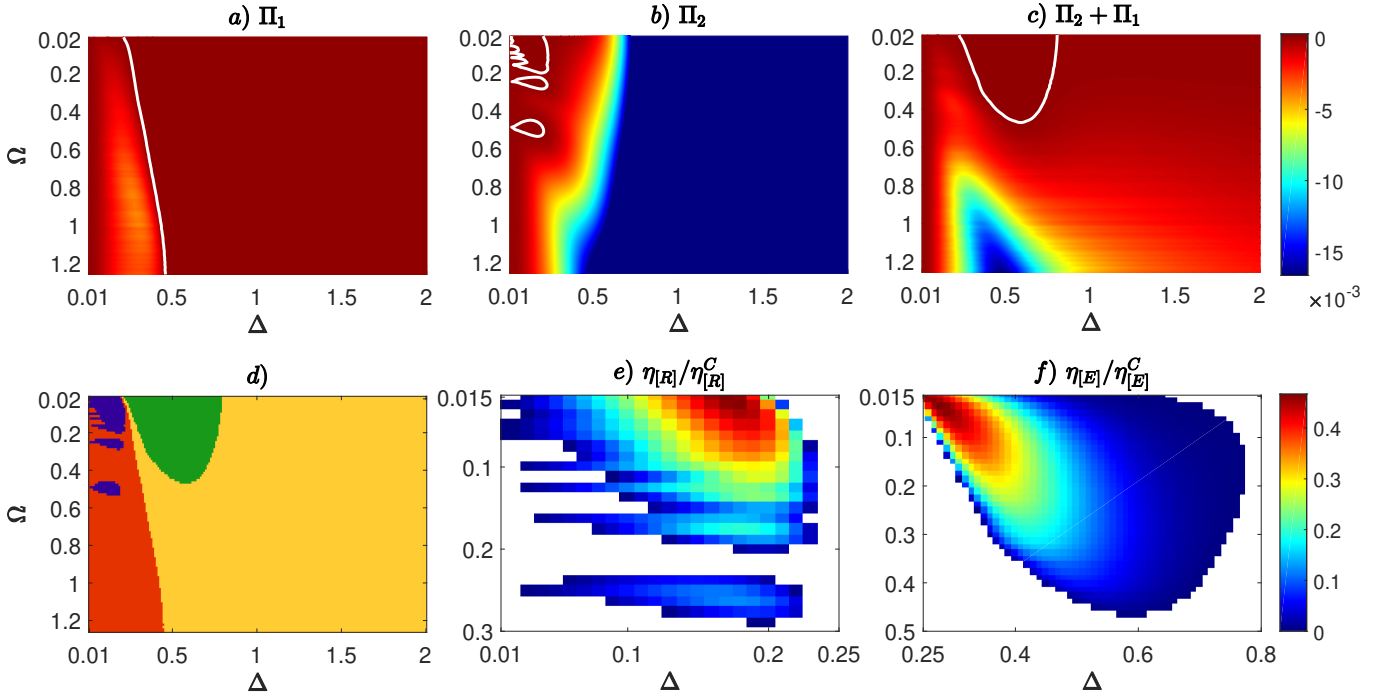


FIG. 7: Same as Fig. 6 but for $\beta_1 E_0 = 1/3$

We present results for the time averaged powers, at steady state, in dimensionless form,

$$\Pi_i = \frac{\hbar}{E_0^2 T} \int_t^{t+T} \Pi_i(s) ds, \quad (45)$$

as a function of Δ and the dimensionless drive frequency $\Omega = 2\pi\hbar f/E_0$ where $T = 1/f$ is the driving period.

In Fig. 6 we plot $\Pi_i, i = 1, 2$, the according power output $\Pi_W = \Pi_1 + \Pi_2$, the operation regions and the [E] and [R] efficiencies (rescaled by the according Carnot efficiencies), as functions of Δ and Ω , for fixed ratio β_1/β_2 . Same in Fig. 7 but for higher temperatures.

Note how some oscillations, signaling the presence of quantum coherences, are present in the low temperature power plots, Fig. (6), while they are washed away in the higher temperature plots, Fig. (7). This effect is analogous to that observed in the ideal case, Figs. (3,4). The oscillations are as well reflected in the plots of the regions of operation resulting in a breakdown of the regions connectedness, see Panel d) of Figs. (6,7).

Inspection of Panels e) and f) of both Fig. 6 and 7 shows, as expected, that the efficiencies grow as the Carnot point is approached, note however that both in the [R] and [E] regions, the maximal efficiency is about half the Carnot efficiency.

Note that, in the large Δ limit, only the [H] operation occurs. While the physics behind this phenomenon can be physically understood based on the previous analysis based on the idealised LZSM dynamics, its emergence can also be seen analytically by taking the large Δ limit of the master equation (43), see Appendix C.

V. REMARKS AND CONCLUSIONS

We have illustrated the emergence of the 4 operation modes allowed by the laws of thermodynamics, in a single qubit quantum Otto engine operating in finite time. We have begun with a general treatment of the idealised case where thermalisation and generic thermally-insulated strokes are well separated. The geometrical properties of the various operation regions in the $(\omega_2/\omega_1, P)$ space is all encoded into the bath temperatures, where P is the transition probability among the qubit levels during the thermally-insulated strokes, and $\omega_{1,2}$ are the qubit level spacings during the thermalisation strokes. Simple analytical expressions have been obtained for the boundaries of the regions. We have then specialised to the case of Landau-Zener-Stückelberg-Majorana dynamics. In this case coherent oscillations break the connectedness of the operation mode regions in the parameter space (Δ, v) .

We then investigated the realistic engine proposed by Karimi and Pekola [15]. We have, accordingly, provided a fully fledged characterisation of the operation of that device in its parameter space (Δ, Ω) , which constitute a solid basis for its design and practical realisation.

The study of the idealised Landau-Zener-Stückelberg-Majorana (LZSM- in short) dynamics provides a good guide to understand its physics through an exactly solvable simplified model. In the realistic case of Karimi and Pekola, coherent effects are less evident than in the idealised LZSM case, which is probably a consequence of a smoother driving (rather than of the continuous interaction with the baths [15]).

We remark that the connectedness of the operation mode regions is important because it is associated with the robustness of the engine operation against experimental noise on the control parameters. In this regard our work corroborates the finding of Karimi and Pekola [15] that operation at too low temperature values might be hindered by coherences. We also noted that despite with increasing energy gap $E_0\Delta$ the quantum adiabatic approximation gets better and better, the engine tends to become a mere heater as $\Delta \rightarrow \infty$ limit, and have explained the origin of this phenomenon.

Appendix A: Operation modes allowed by Clausius inequality for the two-baths case

Eqs. (1, 3), combined with the convention

$$0 < \beta_1 < \beta_2 \quad (A1)$$

are incompatible with four sign combinations for Q_1, Q_2, W .

The case $W > 0, Q_1 < 0, Q_2 < 0$ is not allowed because if $Q_1 > 0, Q_2 > 0$, then, by Eqs. (3,A1), it must be $W > 0$.

The case $W < 0, Q_1 > 0, Q_2 > 0$ is not allowed because if $Q_1 > 0, Q_2 > 0$, then, by Eqs. (3,A1), it must be $W > 0$.

The above two cases are not consistent with energy conservation, Eq. (3).

Regardless of the sign of Q_1 , the case $W > 0, Q_2 > 0$ is incompatible with the Clausius inequality (2). In fact assuming $W > 0, Q_2 > 0$ it is, since $\beta_1 > 0, 0 < \beta_1 Q_1 + \beta_1 Q_2 < \beta_1 Q_1 + \beta_2 Q_2$, because of Eq. (A1), which is in disagreement with Eq. (2), hence both the case $W > 0, Q_1 > 0, Q_2 > 0$, and the case $W > 0, Q_1 < 0, Q_2 > 0$ are not allowed. This reflects the impossibility of having a machine that is at the same time a heat engine (i.e., a work provider $W > 0$) and a refrigerator ($Q_2 > 0$).

No incompatibility exists for the remaining four cases listed in Eqs. (4,5,6,7).

Appendix B: Clausius inequality for an ideal one-qubit quantum Otto engine

Setting $\hbar\omega_1\beta_1/2 = x, \hbar\omega_2\beta_2/2 = y$, the Clausius sum $\Sigma = \beta_1 Q_1 + \beta_2 Q_2$, reads, with $Q_{1,2}$ from Eqs. (27,28):

$$\Sigma = -y \tanh y - x \tanh x + (2P - 1)(y \tanh x + x \tanh y) \quad (B1)$$

Since $x, y \geq 0$, it is $\tanh x \geq 0, \tanh y \geq 0$, hence $y \tanh x + x \tanh y \geq 0$. Since $2P - 1 \leq 1$, it is $(2P - 1)(y \tanh x + x \tanh y) \leq (y \tanh x + x \tanh y)$. Therefore:

$$\begin{aligned} \Sigma &\leq -y \tanh y - x \tanh x + y \tanh x + x \tanh y \\ &= (y - x)(\tanh x - \tanh y) \leq 0 \end{aligned} \quad (\text{B2})$$

where the last inequality follows from the fact that the hyperbolic tangent is a monotonously increasing function. Note that Σ vanishes, that is it gets its largest possible value, at the Carnot point $x = y, P = 1$ (namely $\omega_1 \beta_1 = \omega_2 \beta_2, P = 1$).

Appendix C: Master equation in the large Δ limit

In this appendix we solve the master equation describing the open qubit evolution in the limit $\Delta \gg 1$. This will illustrate the mechanism underling the fact that in the large Δ region of parameters only the heater [H] operation is possible even if the adiabatic approximation is better achieved when Δ gets larger. The transition rates $\Gamma_{\downarrow(\uparrow),j}$ read with the Δ dependence made explicit

$$\begin{aligned} \Gamma_{\downarrow,1} &= A_1 \frac{\Delta^2}{q^2 + \Delta^2} \left| 1 + \mathcal{Q}_1 \left(\sqrt{\frac{q^2 + \Delta^2}{\bar{q}^2 + \Delta^2}} - \sqrt{\frac{\bar{q}^2 + \Delta^2}{q^2 + \Delta^2}} \right) \right|^{-2} \\ &\quad \times \frac{\sqrt{q^2 + \Delta^2}}{1 - e^{-2E_0\beta_1}\sqrt{q^2 + \Delta^2}} \end{aligned} \quad (\text{C1})$$

$$\begin{aligned} \Gamma_{\downarrow,2} &= A_2 \frac{\Delta^2}{q^2 + \Delta^2} \left| 1 + \mathcal{Q}_2 \left(\frac{\sqrt{q^2 + \Delta^2}}{\Delta} - \frac{\Delta}{\sqrt{q^2 + \Delta^2}} \right) \right|^{-2} \\ &\quad \times \frac{\sqrt{q^2 + \Delta^2}}{1 - e^{-2\beta_2 E_0}\sqrt{q^2 + \Delta^2}} \end{aligned} \quad (\text{C2})$$

$$\begin{aligned} \Gamma_{\uparrow,1} &= -A_1 \frac{\Delta^2}{q^2 + \Delta^2} \left| 1 + \mathcal{Q}_1 \left(\sqrt{\frac{q^2 + \Delta^2}{\bar{q}^2 + \Delta^2}} - \sqrt{\frac{\bar{q}^2 + \Delta^2}{q^2 + \Delta^2}} \right) \right|^{-2} \\ &\quad \times \frac{\sqrt{q^2 + \Delta^2}}{1 - e^{2E_0\beta_1}\sqrt{q^2 + \Delta^2}} \end{aligned} \quad (\text{C3})$$

$$\begin{aligned} \Gamma_{\uparrow,2} &= -A_2 \frac{\Delta^2}{q^2 + \Delta^2} \left| 1 + \mathcal{Q}_2 \left(\frac{\sqrt{q^2 + \Delta^2}}{\Delta} - \frac{\Delta}{\sqrt{q^2 + \Delta^2}} \right) \right|^{-2} \\ &\quad \times \frac{\sqrt{q^2 + \Delta^2}}{1 - e^{2\beta_2 E_0}\sqrt{q^2 + \Delta^2}} \end{aligned} \quad (\text{C4})$$

where q is a shorthand for $q(t)$, $\bar{q} = \max q(t)$ and A_1 and A_2 are factors with the dimension of frequency, that contain information about the two resonators and the qubit energy scale E_0 . Performing a Taylor expansion

up to the leading order in $1/\Delta$ we obtain

$$\begin{aligned} \Gamma_{\downarrow,1} &\simeq A_1 \Delta \left(1 - \frac{1}{2} \left(\frac{q}{\Delta} \right)^2 \right) \times \\ &\quad \left(1 + 2\mathcal{Q}_1 \frac{(\bar{q}^2 - q^2)}{\Delta^2} \right) (1 + e^{-2E_0\beta_1\Delta}) \simeq A_1 \Delta \end{aligned} \quad (\text{C5})$$

$$\begin{aligned} \Gamma_{\downarrow,2} &\simeq A_2 \Delta \left(1 - \frac{1}{2} \left(\frac{q}{\Delta} \right)^2 \right) \times \\ &\quad \left(1 - 2\mathcal{Q}_2 \left(\frac{q}{\Delta} \right)^2 \right) (1 + e^{-2\beta_2 E_0\Delta}) \simeq A_2 \Delta \end{aligned} \quad (\text{C6})$$

$$\begin{aligned} \Gamma_{\uparrow,1} &\simeq -A_1 \Delta \left(1 - \frac{1}{2} \left(\frac{q}{\Delta} \right)^2 \right) \times \\ &\quad \left(1 + 2\mathcal{Q}_1 \frac{(\bar{q}^2 - q^2)}{\Delta^2} \right) e^{-2E_0\beta_1\Delta} \simeq -A_1 \Delta e^{-2E_0\beta_1\Delta} \end{aligned} \quad (\text{C7})$$

$$\begin{aligned} \Gamma_{\uparrow,2} &\simeq -A_2 \Delta \left(1 - \frac{1}{2} \left(\frac{q}{\Delta} \right)^2 \right) \times \\ &\quad \left(1 - 2\mathcal{Q}_2 \left(\frac{q}{\Delta} \right)^2 \right) e^{-2\beta_2 E_0\Delta} \simeq -A_2 \Delta e^{-2\beta_2 E_0\Delta} \end{aligned} \quad (\text{C8})$$

The master equations for the time evolution of ρ_{gg} and ρ_{ge} then reads

$$\begin{aligned} \dot{\rho}_{gg}(t) &= -\frac{\Delta}{q^2(t) + \Delta^2} \dot{q}(t) \Re[\rho_{ge}(t)e^{i\phi(t)}] - \Gamma_{\Sigma} \rho_{gg}(t) + \Gamma_{\downarrow} \\ &\simeq (A_1 + A_2) \Delta (1 - \rho_{gg}) \end{aligned} \quad (\text{C9})$$

$$\begin{aligned} \dot{\rho}_{ge}(t) &= \frac{\Delta}{q^2(t) + \Delta^2} \dot{q}(t) (\rho_{gg}(t) - 1/2) e^{-i\phi(t)} - \Gamma_{\Sigma} \rho_{ge}(t)/2 \\ &\simeq -(A_1 + A_2) \Delta \rho_{ge}/2 \end{aligned} \quad (\text{C10})$$

where $\Gamma_{\Sigma} = \Gamma_{\downarrow,1} + \Gamma_{\downarrow,2} + \Gamma_{\uparrow,1} + \Gamma_{\uparrow,2} \simeq (A_1 + A_2) \Delta$ and $\Gamma_{\downarrow} = \Gamma_{\downarrow,1} + \Gamma_{\downarrow,2} \simeq (A_1 + A_2) \Delta$ and the first terms on the right hand side of both equations have been neglected because they are of order $1/\Delta$ while all the other terms are of order Δ . In this limit the two equations are no more coupled and they can be easily solved:

$$\rho_{gg}(t) \simeq 1 - (1 - \rho_{gg}(0)) e^{-\Delta(A_1 + A_2)t} \quad (\text{C11})$$

$$\rho_{ge}(t) \simeq \rho_{ge}(0) e^{-\Delta(A_1 + A_2)t/2} \quad (\text{C12})$$

In our case the initial state of the qubit at $t = 0$ is a thermal state at reverse temperature β_1 and when $\Delta \gg 1$ it becomes

$$\begin{aligned} \rho_{gg}(0) &= \frac{e^{E_0\beta_1\sqrt{q^2 + \Delta^2}}}{\cosh(E_0\beta_1\sqrt{q^2 + \Delta^2})} \simeq \frac{1}{1 + e^{-2E_0\beta_1\Delta}} \\ &\simeq 1 - e^{-2E_0\beta_1\Delta} \end{aligned} \quad (\text{C13})$$

$$\rho_{ge}(0) \simeq 0 \quad (\text{C14})$$

Substituting (C13) and (C14) into equation (C11) and (C12) respectively we obtain

$$\rho_{gg}(t) \simeq 1 - e^{-\Delta(E_0\beta_1 + (A_1 + A_2)t)} \quad (\text{C15})$$

$$\rho_{ge}(t) \simeq 0 \quad (\text{C16})$$

We note that for $\Delta \rightarrow \infty$ it is $\rho_{gg} \rightarrow 1$. Accordingly the qubit tends to stay in its ground state for all t 's and this effect is more evident for larger β_1 (smaller temperatures). The expression for instantaneous dimensionless power Π_j to resistor j reads

$$\begin{aligned} \Pi_j(t) &= 2(\hbar/E_0)\sqrt{q^2 + \Delta^2}(\Gamma_{\downarrow,j} - \rho_{gg}(\Gamma_{\downarrow,j} + \Gamma_{\uparrow,j})) \\ &\simeq 2(\hbar/E_0)\Delta \left(A_j\Delta - \left(1 - e^{-\Delta(E_0\beta_1 + (A_1 + A_2)t)}\right) A_j\Delta \right) \\ &\simeq 2(\hbar/E_0)A_j\Delta^2 e^{-\Delta(E_0\beta_1 + (A_1 + A_2)t)} \geq 0 \end{aligned} \quad (\text{C17})$$

Hence the dimensionless average value of power over a period T of the driving become

$$\begin{aligned} \Pi_j &\simeq \frac{2\hbar A_j \Delta^2}{E_0 T} \int_0^T e^{-\Delta(E_0\beta_1 + (A_1 + A_2)s)} ds \\ &= \frac{2\hbar A_j}{E_0^2 T} \frac{(1 - e^{-E_0\beta_1\Delta(A_1 + A_2)T})}{\beta_1(A_1 + A_2)} \Delta e^{-E_0\beta_1\Delta} \\ &\simeq \frac{2\hbar}{E_0^2 T} \frac{A_j}{A_1 + A_2} \frac{\Delta}{\beta_1} e^{-E_0\beta_1\Delta} \geq 0 \end{aligned} \quad (\text{C18})$$

Accordingly in the large Δ limit, both the powers to resistors are positive and consequently the only possible regime is the heater [H].

-
- [1] E. Fermi, *Thermodynamics* (Dover, New York, 1956).
[2] L. Buffoni, A. Solfanelli, P. Verrucchi, A. Cuccoli, and M. Campisi, Phys. Rev. Lett. **122**, 070603 (2019).
[3] D. Schmidtke, L. Knipschild, M. Campisi, R. Steinigeweg, and J. Gemmer, Phys. Rev. E **98**, 012123 (2018).
[4] A. W. Marshall, I. Olkin, and B. C. Arnold, *Inequalities: Theory of Majorization and its Applications*, vol. 143 (Springer, 2011), 2nd ed.
[5] A. Messiah, *Quantum Mechanics* (North Holland, Amsterdam, 1962).
[6] H. Quan, Y.-x. Liu, C. Sun, and F. Nori, Phys. Rev. E **76**, 031105 (2007).
[7] A. del Campo, J. Goold, and M. Paternostro, Sci. Rep. **4** (2014).
[8] L. D. Landau, Phys. Z. Sowjetunion **2**, 46 (1932).
[9] C. Zener, Proc. R. Soc. A **137**, 696 (1932).
[10] E. C. G. Stückelberg, Helv. Phys. Acta **5**, 369 (1932).
[11] E. Majorana, Il Nuovo Cimento (1924-1942) **9**, 43 (1932).
[12] N. V. Vitanov and B. M. Garraway, Phys. Rev. A **53**, 4288 (1996).
[13] I. M. J. A. Z. D. Gradshteyn, I. S.; Ryzhik, *Table of Integrals, Series, and Products* (Elsevier Academic Press, 2007).
[14] N. V. Vitanov, Phys. Rev. A **59**, 988 (1999).
[15] B. Karimi and J. P. Pekola, Phys. Rev. B **94**, 184503 (2016).
[16] M. Campisi, P. Hänggi, and P. Talkner, Rev. Mod. Phys. **83**, 771 (2011), *ibid.* p. 1653.
[17] Usually one assumes K to be the time-reversal operator [16], but that is not necessary for our purposes.